Geophysical Research Letters

RESEARCH LETTER
10.1029/2018GL077343

Controls on Early-Rift Geometry: New Perspectives From the Bilila-Mtakataka Fault, Malawi

M. Hodge[1], Å. Fagereng[1], J. Biggs[2], and H. Mdala[3]

[1]School of Earth and Ocean Sciences, Cardiff University, Cardiff, UK, [2]School of Earth Sciences, University of Bristol, Bristol, UK, [3]Geological Survey Department, Mzuzu Regional Office, Mzuzu, Malawi

Key Points:
- The segmented 110-km long Bilila-Mtakataka fault scarp is oriented oblique to the current regional extension direction
- The surface expression is compatible with the upward propagation of a buried weak zone that fits the local stress field
- High-grade metamorphic foliation locally influences scarp trend at the surface

Supporting Information:
- Supporting Information S1

Correspondence to:
M. Hodge,
hodgems@cardiff.ac.uk

Citation:
Hodge, M., Fagereng, Å., Biggs, J., & Mdala, H. (2018). Controls on early-rift geometry: New perspectives from the Bilila-Mtakataka fault, Malawi. *Geophysical Research Letters*, *45*, 3896–3905. https://doi.org/10.1029/2018GL077343

Received 29 JAN 2018
Accepted 25 MAR 2018
Accepted article online 20 APR 2018
Published online 5 MAY 2018

Abstract We use the ~110-km long Bilila-Mtakataka fault in the amagmatic southern East African Rift, Malawi, to investigate the controls on early-rift geometry at the scale of a major border fault. Morphological variations along the 14 ± 8-m high scarp define six 10- to 40-km long segments, which are either foliation parallel or oblique to both foliation and the current regional extension direction. As the scarp is neither consistently parallel to foliation nor well oriented for the current regional extension direction, we suggest that the segmented surface expression is related to the local reactivation of well-oriented weak shallow fabrics above a broadly continuous structure at depth. Using a geometrical model, the geometry of the best fitting subsurface structure is consistent with the local strain field from recent seismicity. In conclusion, within this early-rift, preexisting weaknesses only locally control border fault geometry at subsurface.

Plain Language Summary This study investigates the controls to fault and rift geometry for a young rift system. Our case study is a large fault in southern Malawi. The geometry of the fault at the surface, the scarp and structures within the rocks the fault cuts through, is measured. We also calculate the scarp height. The orientation and height of the fault scarp implies that local stresses influence its geometry, not regional stresses. We develop a geometrical model to link the scarp and a fault at depth. The best fit model is consistent with the hypothesis that the local stress influences the current fault geometry. We propose that a weak zone at depth may also influence the fault geometry, but weaknesses near the surface only locally influence fault orientation.

1. Introduction

Rift structure is controlled by the geometry of border faults. In intact, isotropic rocks, normal border faults would strike perpendicular to the least principal stress and dip 60°. Frictionally weak and/or low cohesive strength caused by preexisting structures can, however, localize strain and provide surfaces for fault reactivation (e.g., Bellahsen et al., 2013; Walker et al., 2015; Worthington & Walsh, 2016), including structures that are not ideally oriented in the current stress field (e.g., Ebinger et al., 1987). Therefore, preexisting structures formed in both current and previous deformation phases can have a fundamental influence on rift geometry (e.g., Phillips et al., 2016; Whipp et al., 2014). For young rifts where the initial structure is currently being established, such as parts of the East African Rift System (Macgregor, 2015), prerift structures such as basement foliations, or structures originating from older rift events, have been suggested as primary controls on the current rift geometry and evolution (Corti, 2009; Delvaux et al., 2012; Morley, 2010). However, alternative hypotheses suggest that early rifting is controlled by the stress field at the time of fault nucleation (Fazlikhani et al., 2017; McClay & Khalil, 1998), anisotropy in the lithospheric mantle (Tommasi & Vauchez, 2001), or thermal weakening (Claringbould et al., 2017).

As well as rift-scale observations, the influence of preexisting structures has been demonstrated in laboratory rock deformation (e.g., Collettini et al., 2009) and analog experiments (e.g., Bellahsen & Daniel, 2005), yet, over the scale of an individual fault their influence is less clear (e.g., Phillips et al., 2016; Whipp et al., 2014). An expectation is that a major fault is either parallel to reactivated weak surfaces or in an orientation consistent with fault nucleation in the current stress field. In the Suez Rift, a combination of these options is illustrated by foliation-oblique faults reflecting the stress at fault initiation, hard linked by foliation-parallel faults (McClay & Khalil, 1998).

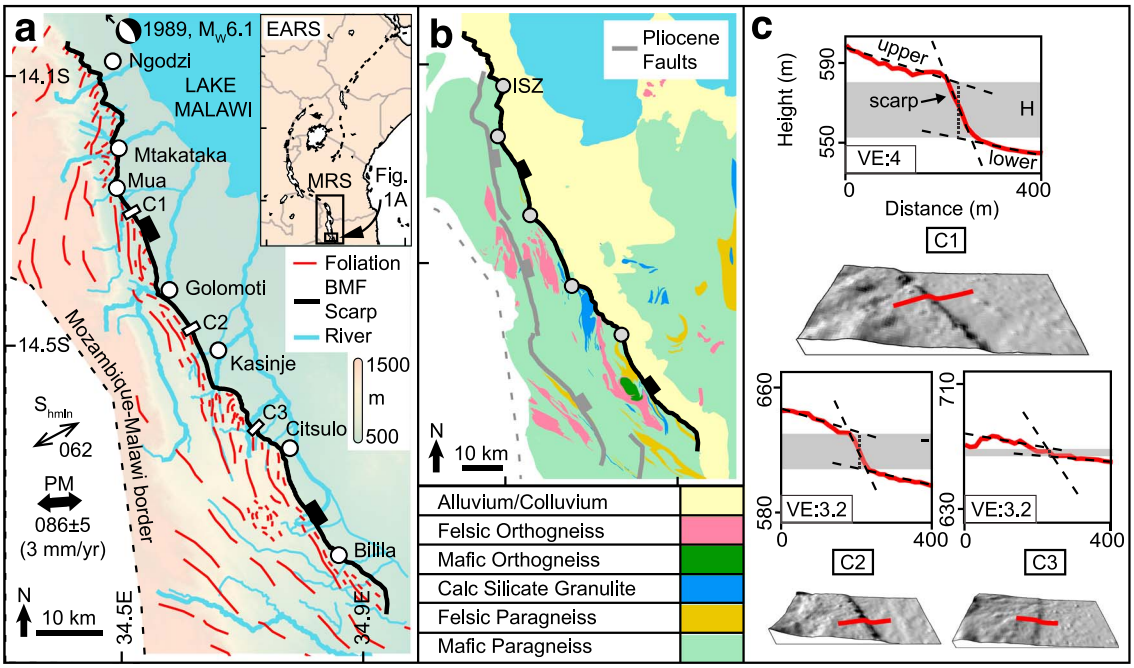

Figure 1. (a) Geographical context of the Bilila-Mtakataka fault (BMF) scarp. S_{hmin} = minimum horizontal stress from Delvaux and Barth (2010); PM = current regional extension direction from Saria et al. (2014); EARS = East African Rift System; MRS = Malawi Rift System. For a map of the main structural features along the EARS please see Figure S2 in the supporting information. (b) Geological map modified after Walshaw (1965) and Dawson and Kirkpatrick (1968). Light gray-filled circles denote inferred intersegment zones (ISZ, Figure 2). (c) Elevation profiles and hillshade digital elevation models; numbers refer to locations in panel A. Definitions of upper and lower surfaces and the method for deriving scarp height, *H*; follow Avouac (1993). Vertical exaggeration (VE) is displayed on the profiles.

Here we address the relative importance of the controls on rift and fault geometry, by using high-resolution satellite and field measurements to describe the geometry of the Bilila-Mtakataka fault (BMF) and foliations in the crystalline footwall rocks (Figure 1a). The BMF is a normal border fault at the southern end of the amagmatic Malawi Rift System, whose surface trace has been suggested to comprise a continuous ~10-m high scarp for ~100 km (Jackson & Blenkinsop, 1997). Rift initiation in the southern Malawi Rift System may be as recent as early to middle Pliocene (Lyons et al., 2011), so the BMF provides a rare natural laboratory for the relationship between basement foliation and fault geometry in the early stages of rifting. We discuss whether BMF geometry is consistent with basement reactivation, stresses inferred from regional extension, and/or a different local stress field at the time of initiation. With the availability of this data set, we also aim to provide new insights into the morphology of one of the Earth's longest, continental normal fault scarps.

2. Data Collection and Methodology

We analyze a 12-m resolution TanDEM-X digital elevation model (DEM) using QGIS to calculate scarp height and width from elevation profiles along the BMF scarp at 1-km intervals (Figure 1c). The BMF scarp was mapped at 1:100 scale from 14.04°S, 34.34°E to 14.93°S, 34.94°E; 128 profiles were extracted, each with a length of 400 m. As the slip direction is considered to be pure normal (Chorowicz & Sorlien, 1992; Jackson & Blenkinsop, 1997), elevation profiles were oriented perpendicular to the local scarp trend. Previous regional fault studies in Malawi have used a 30-m Shuttle Radar Topography Mission (SRTM) DEM to map faults (e.g., Laó-Dávila et al., 2015); however, TanDEM-X is higher resolution and has higher absolute and relative vertical accuracies (e.g., Gruber et al., 2012). Here for a subsample of 50 control points, the median difference between the TanDEM-X DEM and an SRTM DEM was found to be less than 5 m.

Scarp height is defined as the elevation difference between regression lines fitted to the footwall and hanging wall surfaces, extrapolated to a line through the point of maximum slope on the fault scarp (Figure 1c; Avouac, 1993). To generate the regression lines, the bottom and top of the scarp were picked manually. Measurements were repeated three times in random order to calculate uncertainty. Interpretation of each profile

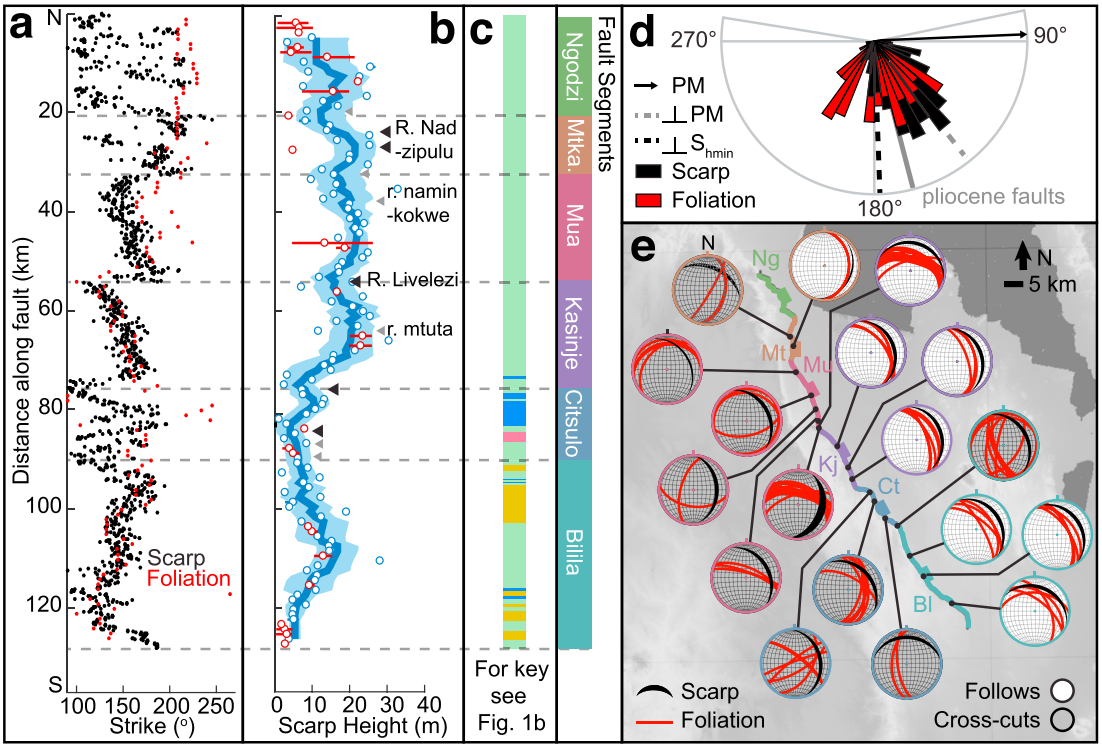

Figure 2. Panels a–c are plots of distance along the Bilila-Mtakataka fault scarp against: (a) scarp trend and foliation strike from digital elevation model and geological maps. (b) Scarp height measured from digital elevation model. Repeatable measurements are blue circles, and nonrepeatable are red circles (error bars included). A 5-km moving average (blue solid line) and standard deviation (blue shaded area) are also given. Black and gray triangles mark major and minor rivers, respectively. (c) Footwall lithology; see Figure 1b for key (Mtka = Mtakataka). (d) Angular relationship between scarp trend (black), foliation strike (red), current regional extension direction (PM, black arrow; from Saria et al., 2014), and planes perpendicular to current regional extension direction (⊥PM, black dotted line) and to local minimum horizontal stress ($\perp Sh_{min}$, gray dotted line; from Delvaux & Barth, 2010). (e) Map of BMF segments (colored: Ng = Ngodzi; Mt = Mtakataka; Mu = Mua; Kj = Kasinje; Ct = Citsulo; and Bl = Bilila), including lower hemisphere, equal angle, stereoplots showing field measurements of scarp, and basement rock foliation, indicating where the scarp follows (white) or crosscuts (gray) local foliation.

can be found in the supporting information. The root mean square error (RMSE) for the regression lines was on average ~1.5 m (Table S2 in the supporting information), and the standard deviation of errors between measurements was ~0.4 m (red circles, Figure 2b). Measurement repeatability (here defined as horizontal error between all scarp picks of less than 10 m) was achieved for 102 of the 128 profiles (blue circles, Figure 2b), with fewer repeatable measurements at the ends of the fault where the scarp is smaller and therefore more difficult to recognize in the DEM (Figure 2b). To reduce measurement errors or other local site effects (e.g., erosion; Zielke et al., 2015), 5-km moving average and standard deviation are applied to the repeatable measurements (blue line and envelope, Figure 1b).

In the field, the scarp is expressed as a soil-mantled hillslope. Bedrock exposures are scattered, and there are no known exposures where displacement can be directly measured across the fault. No fault plane slip direction indicators unequivocally formed by rift-related faulting were found. Dip and dip azimuth of the scarp slope were measured at 17 locations (Figure 2e), but note that given the weathered, soil-dominated nature of the scarp, the dip is representative of the angle of repose and may be less than the dip of the fault plane. Thus, whereas the uncertainty in the absolute dip measurements is ~5°, this dip may differ significantly from fault plane dip. Basement foliation orientation was also measured in the footwall amphibolite to granulite facies gneisses at each location and augmented by interpolation of composition and fabric orientations from geological maps (Figure 1b; Dawson & Kirkpatrick, 1968; Walshaw, 1965). The mineralogy of the gneisses is dominated by biotite, feldspar, and quartz in variable modal proportions, with smaller but variable modes of hornblende and garnet. The gneissic foliation is continuous, cohesive, and typically planar, but locally anastomosing, and defined by both mineral segregation banding and preferred mineral orientations.

3. Results

3.1. Scarp Morphology and Segmentation

Analysis of the TanDEM-X DEM shows that the trend of the BMF scarp is locally variable, with an average of ~150° (Figure 2a). This average trend is at an angle of 64° to the current regional plate motion vector estimate of 086° ±5° (Saria et al., 2014, Figure 2d). On the other hand, this average scarp trend is 88° to a local, minimum horizontal stress (Sh_{min}) inferred from 13 earthquake focal mechanisms in the Malawi rift (Delvaux & Barth, 2010, Figure 2d). The footwall basement foliation has a bimodal strike distribution with peaks at 160° and 205° but varies considerably along the BMF (Figure 2a).

The average scarp height is 14 m (σ = 8 m) but varies by an average of 6 m/km; the largest measured scarp height is ~34 m (Figure 2b). Only minor changes in scarp morphology occur at major rivers. The scarp height displays two bell-shaped, near-symmetrical profiles; one in the north (0 ~ 80 km) and one in the south (95 ~ 128 km). Between 80 and 95 km, scarp height is almost 0 and the scarp trend varies considerably, forming two bends around surface exposures of calc-silicate granulite (Figures 1b and 2c). Based on major gaps in fault scarp continuity or distinct along-strike changes in scarp morphology and/or scarp trend (e.g., Crone & Haller, 1991), the BMF can be divided into six segments (Figure 2 and Table S1). These segments are now described from north to south.

3.2. Structural Analysis of BMF Segments

In the northernmost segment, Ngodzi, the fault scarp orientation alternates in a zigzag pattern between a predominant trend of 110°, which crosscuts gneissic foliations, and a foliation-parallel trend of 210°, where the scarp is steepest. For the northernmost few kilometers, a scarp is not obvious on the DEM profiles, but then a scarp of 13 ± 8 m can be traced (Figure 2b).

Along the Mtakataka segment an 18 ± 5-m high scarp is subparallel to the eastward dipping foliation (dip 48° ±22°, Figure 2e), except at the river Nadzipulu where the scarp (locally 25-m high) crosscuts the foliation to trend ~120° for 2 km. As in the Ngodzi segment, the scarp dips more gently (~30°) where the scarp and foliation are subparallel than where the scarp crosscuts the foliation (~40°, Figure 2e).

The Mua segment is convex in shape, consistently oblique to the foliation, and its trend rotates southwestward from 150° to 200° at 2°/km (Figure 2a). Scarp height is 20 ± 6 m and decreases slightly at both ends of the segment (Figure 2b). Toward the northern end, at the Naminkokwe river, a 13-m high knickpoint has eroded back 70 m, and a number of steeply dipping extensional fractures, likely associated with recent fault-related deformation, strike parallel to the scarp and crosscut the gently dipping foliation (Figures 3a–3c). The Mua segment intersects the Kasinje segment at the river Livelezi, where the scarp abruptly rotates from trending 185° to a trend of 115° (Figure 2a). This change coincides with an increase in scarp dip to 45° (Figure 2e).

In contrast to the Mua segment, the entire Kasinje segment is parallel to foliation that dips eastward at 53° ± 9° (Figures 2a and 2e). The scarp is concave in map view, and scarp trend and foliation strike both increase southward by around 2°/km. The scarp is clearly defined with an average height of 16 ± 8 m, reaching a maximum of 24 m near the segment center. A 16-m high knickpoint in the Mtuta river is set back 40 m from the scarp front and shows that the fault is parallel to the local foliation and lacks a fractured footwall damage zone (Figures 3d–3f). Scarp height decreases to less than 10 m several kilometers from the intersection with the Citsulo segment.

The Citsulo segment has an irregular scarp trend that alternates between ~120° and ~185°. The scarp trace forms two large, approximately right angle bends (Figure 1a). In the field, the scarp can be traced around both bends; however, it is difficult to identify the fault scarp from the hills behind it between these features. Although two <10-m high north-south trending scarps can be identified in the DEM, they are offset by several kilometers (Figure 2b). This is the only discontinuity of the scarp trace along the entire surface length of the BMF, and we define this as the "Citsulo discontinuity." The footwall lithology is more variable here than elsewhere along the fault and comprises intercalated bands of felsic orthogneisses, mafic paragneisses, and calc-silicate granulite (Figure 2c), with a steeply dipping (62° ± 13°), variably folded and locally discontinuous foliation.

The southernmost segment, Bilila, has a concave scarp parallel to strike of foliations that dip eastward at 53° ± 19°. A scarp of height 9 ± 6 m can be seen along the entire segment before the scarp becomes indistinguishable on the DEM after 120 km. Lithology along the Bilila segment varies between a volumetrically dominant mafic paragneiss unit and bands of calc-silicate granulite and felsic paragneisses.

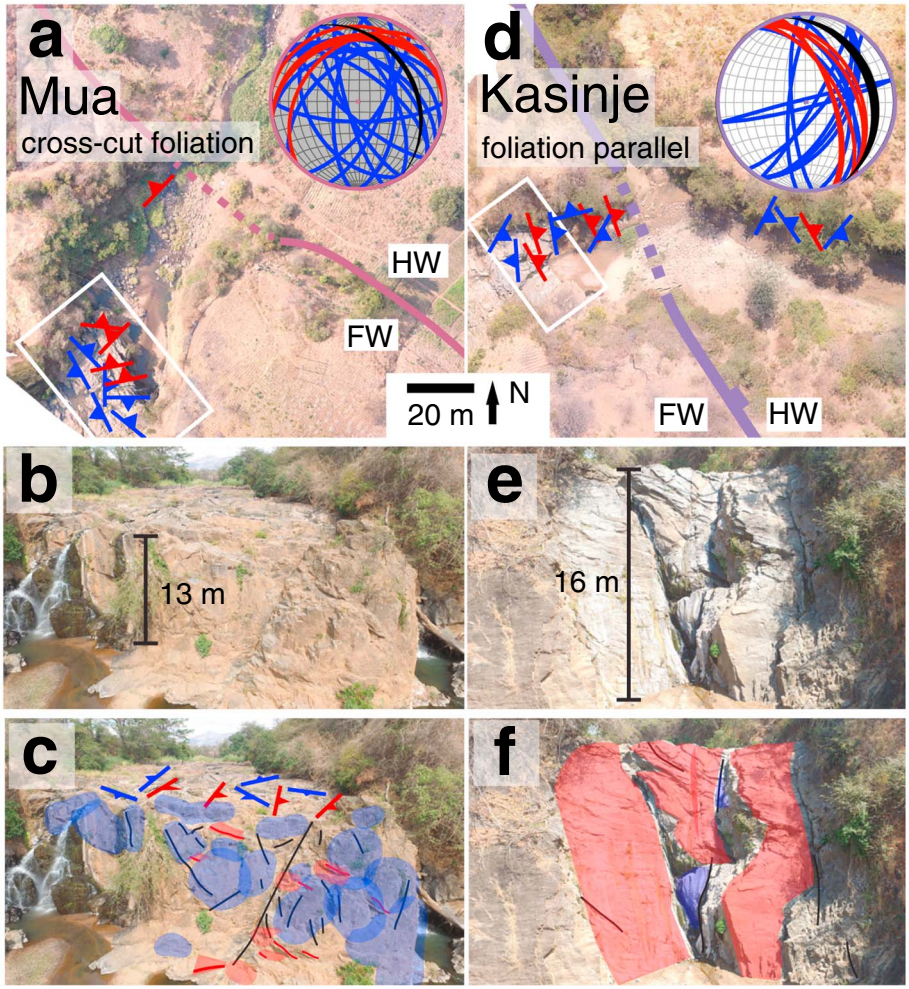

Figure 3. Photographs of (a) Mua and (d) Kasinje knickpoints showing foliation (red) and fracture (blue) orientations from (b/e) above and on the (c/f) waterfall. For (c/f), where the waterfall is parallel to a foliation or a fracture surface, the surface is colored appropriately (i.e., red or blue). Foliation dips much more gently at Mua than Kasinje. The scarp trend and waterfall surface at the Mua knickpoint (set back 70 m from the scarp) crosscut the high-grade metamorphic foliation, whereas both are parallel to foliation at the Kasinje knickpoint that is set back 40 m from the fault scarp.

4. Discussion

4.1. Variations in Scarp Trend

The total length of the surface fault trace where a scarp was identified in the DEM is ~110 km. The along-strike profile of scarp height displays two bell-shaped profiles and comprises several peaks and troughs indicative of fault segmentation (e.g., Crider & Pollard, 1998; Crone & Haller, 1991; Walker et al. 2015, Figure 2b). Segmented, but bell-shaped scarp height profiles generally result from hard links between initially independent segments (e.g., Anders & Schlische, 1994; Dawers & Anders, 1995; Trudgill & Cartwright, 1994) and interactions with other structures or strength anisotropies (e.g., Fossen & Rotevatn, 2016). An increase in scarp dip at intersegment zones along the fault (e.g., between the Mua and Kasinje segments) may also be due to hard links established by progressive growth of secondary faults, such as breached relay ramps or transfer faults (e.g., Gawthorpe & Hurst, 1993; Peacock, 2002; Trudgill & Cartwright, 1994).

Scarp height on the Citsulo segment is too low to fit a bell-shaped height curve to the entire fault scarp (Figure 2b). This low height, and the observation that the scarp is discontinuous near Citsulo, may indicate that the BMF comprises two separate faults. In this interpretation, there is no hard link between a 65-km long northern fault comprising the four segments north of Citsulo and a 30-km long southern fault represented by the Bilila segment.

Similar to other faults whose surface trace is discontinuous, the BMF may be continuous at depth (e.g., Nicol et al., 2005; Worthington & Walsh, 2016). Note, however, that the low scarp height in the Citsulo segment may be related to local change in surface lithology. Whereas the majority of the fault displaces foliated, biotite-bearing gneisses, the scarp at Citsulo bends around poorly foliated, diopside-tremolite calc-silicate granulite, which is both frictionally strong (He et al., 2013) and lacks any preexisting weak planes.

The BMF scarp parallels the strike of local foliation along 60% of its length (Figure 2a). Where the scarp locally bends to crosscut the foliation, for example, Ngodzi and Mtakataka, such bends form high-angle links between en echelon foliation-parallel scarps. These bends create a zigzag pattern similar to other faults that locally reactivate weak planes (e.g., Bellahsen & Daniel, 2005; McClay & Khalil, 1998), except that the cross-foliation segments do not have a consistent strike (Figure 2a). The only major segment that crosscuts foliation along its full length is Mua, where foliation dips more gently than elsewhere along the scarp. This corroborates existing hypotheses that gently dipping structures are difficult to frictionally reactivate in rifts (e.g., Collettini & Sibson, 2001; Phillips et al., 2016). On the Ngodzi and Mtakataka segments, the scarp is steeper where it crosscuts the foliation, and a more gentle scarp is also present on the foliation-parallel Kasinje segment, compared to the Mua segment. While to the first order, the BMF scarp systematically appears steeper where it crosscuts foliation, a combination of factors including erosion rate, scarp age, footwall damage zone parameters, and original scarp shape influences the current scarp slope (Arrowsmith et al., 1998; Avouac, 1993), and the interpretation of this tentative relation between scarp slope and foliation orientation is highly uncertain.

4.2. Relations Between Fault Scarp Geometry, Local and Regional Stresses, and Preexisting Structures

The average trend of the BMF scarp is comparable to the strike of the nearest instrumentally recorded earthquake, the 1989 Salima M_W 6.1 event (strike 154° ± 25°, dip 32° ± 5°, and rake −92° ± 25°), whose epicenter was ~ 40 km from the northern tip of the BMF scarp (Jackson & Blenkinsop, 1993). Whereas a normal fault striking perpendicular to the current plate motion would strike 176° ± 5° (Saria et al., 2014), the BMF average scarp trend fits well with the current local stress field estimated from focal mechanisms (Sh_{min} = 062°; Delvaux & Barth, 2010). This estimate, however, relies on only 13 earthquakes throughout the Malawi rift and could reflect local strain as accommodated on reactivated faults rather than local stress (Twiss & Unruh, 1998). However, reorientation of the local stress field along zones of weak fabric in rifts has been suggested to occur in close proximity to major border faults along the East African Rift System (Corti et al., 2013; Morley, 2010).

The BMF scarp is neither consistently parallel to foliation nor in an orientation expected from current plate motion. We therefore propose that the fault segments are linked within the brittle zone to a deeper structure that controls the average surface trace (Figure 4a). Variations in scarp height are greatest in the north (Figure 2b), where very pronounced zigzags in scarp trend are observed (Figure 2a). We therefore infer that these peaks and troughs in scarp height, which have previously been interpreted as indicators of deeper segmented ruptures (e.g., Cartwright et al., 1996), may in fact result from local variations in fault geometry (e.g., Mildon et al., 2016; Zielke et al., 2015), here caused by heterogeneous reactivation of weak shallow fabrics above a broadly continuous structure. In fact, the local variability in BMF scarp geometry and morphology is similar to other scarps suggested to have formed due to reactivation of a deep structure (e.g., the Egiin Davaa scarp, Mongolia; Walker et al., 2015). Furthermore, the angular relationship between scarp trend and foliation strike at the surface on the BMF is also consistent with field observations by Pennacchioni and Mancktelow (2007), who describe reactivation of deeper structures in the ductile field but that shallower brittle fractures largely crosscut cohesive, metamorphic structures and foliations, except where well oriented. We also note that the foliation-oblique scarp segments, big or small, do not have a consistent trend (Figure 2a), as opposed to what one would expect if a consistent stress field, at the scale of the fault, controlled their orientation. Our findings are similar to those by Kolawole et al. (2018) for northern Malawi, who through field observations and aeromagnetic data suggest that the 2009 Karonga earthquake sequence (Biggs et al., 2010) occurred on a deep structure that reactivated basement fabric. They found that the basement fabric was associated with the Precambrian Mughese Shear Zone, and the strike of the deep structure is oblique to the regional stress field. As inferred here, the deep structure likely caused a rotation of the local stress field, as suggested elsewhere along the East African Rift System (e.g., Corti et al., 2013; Morley, 2010).

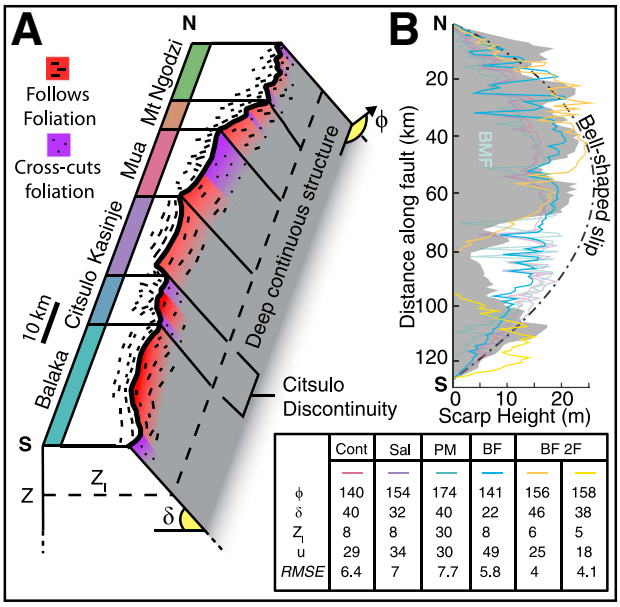

	Cont	Sal	PM	BF	BF 2F	
ϕ	140	154	174	141	156	158
δ	40	32	40	22	46	38
Z_l	8	8	30	8	6	5
u	29	34	30	49	25	18
RMSE	6.4	7	7.7	5.8	4	4.1

Figure 4. (a) Schematic of the Bilila-Mtakataka fault, showing where it follows (red) or crosscuts (purple) the high-grade metamorphic foliation and an inferred link to a deep structure of strike ϕ and dip δ at a linking depth Z_l. (b) Calculated scarp height, *H*, for the current Bilila-Mtakataka fault scarp if it is linked to a deep structure with maximum slip at the center, for various deep structure Z_l, ϕ, δ, maximum slip *u*, and length *L* (Cont = continuous structure that strikes parallel to the average scarp trend; Sal = continuous structure with ϕ and δ from 1989 Salima earthquake; PM = continuous structure with a ϕ perpendicular to the current regional extension direction (taken from Saria et al., 2014); BF = best fitting continuous structure; BF 2F = best fitting scenario with two separate faults at depth). The observed Bilila-Mtakataka fault scarp height is also plotted for comparison (see table for root mean square error [RMSE]). See the supporting information for methodology (Figure S1).

The current scarp height along the BMF may also be evidence of reactivation of a preexisting weakness at depth. As no fault plane slip direction indicators were found, we assume that the faults are purely normal (Chorowicz & Sorlien, 1992; Jackson & Blenkinsop, 1997). Under this assumption the scarp height may be used to represent the surface displacement (Morley, 2002), except where the scarp trend varies considerably from the average trend (Mackenzie & Elliott, 2017). Relative to the fault length, the average vertical surface displacement (~14 m) is greater than would be expected by a single earthquake event (~6 m; Scholz, 2002), but the maximum surface displacement (~28 m) is significantly less than expected for the total displacement (~1,000 m; Kim & Sanderson, 2005). Although surface displacements may be several times less than those at depth (e.g., Villamor & Berryman, 2001), the BMF is still underdisplaced compared to its length. This may suggest that the length of the BMF established rapidly in its slip history, before undergoing a current phase of displacement accumulation, that is, following the constant-length model of fault growth (e.g., Walsh et al., 2002). This fault growth model has been suggested to occur in reactivated fault systems where fault lengths are inherited from underlying structures (Walsh et al., 2002). As such, this morphological analysis of the BMF is consistent with our structural interpretation that the fault is controlled by a preexisting weak zone at depth-oriented oblique to the regional stress direction.

4.3. A Hypothesis Test for a Deep Structure Controlling the Average Surface Fault Trace

To test our deep structure hypothesis, we construct a simple geometrical model to fit an irregular surface between the observed BMF scarp trend and an inferred planar deep structure (Figure S1). Whereas we recognize that this deeper structure may itself be geometrically complex, segmented, or controlled by subsurface fabrics, we assume a planar form for simplicity of this hypothesis test. Slip is projected on the deep, planar structure (assuming a bell-shaped along-strike-slip profile, with constant slip downdip) to the observed surface trace of the scarp (Figure S1e). As no strike-slip offsets were found in the field or on the DEM, we assume that the slip direction on the deep structure is purely normal (Chorowicz & Sorlien, 1992; Jackson & Blenkinsop, 1997). We then use the scarp trend orientation to calculate the vertical throw, and by using this as a proxy for scarp height (e.g., Morewood & Roberts, 2001), we compare against our measurements from the BMF scarp (Figure 4b). We vary strike (ϕ), dip (δ), slip (*u*), and length (*L*) of the inferred structure and the linking depth (Z_l) between this deeper structure and the fault segments observed at the surface.

Fixing the strike of the deep structure to be perpendicular to current plate motion (174°) and dip to be between 40° and 60° requires a linking depth greater than 25 km (RMSE ~ 8 m; Figures S1c and 4b). This linking depth is approximately equal to, or greater than, the inferred fault locking depth in south Malawi (~ 30 km; Jackson & Blenkinsop, 1993) and implies that if the fault formed in the current stress regime, it would exist as a series of discontinuous segments. Inferring a deep structure that strikes subparallel to the average BMF scarp trend (150°) or is parallel to the strike of the 1989 Salima earthquake, however, produces a better match (RMSE 6–7 m) to the observed scarp height with a shallower linking depth (Figure 4b). The best fitting continuous deep structure strikes 141°, dips 22° and requires a linking depth of 8 km and a slip of 49 m (RMSE ~6 m; Figure 4b).

A single, continuous structure with $Z_l \leq 10$ km requires slip > 30 m, significantly more than anticipated in a single rupture (Scholz, 2002), but could represent cumulative slip from several events. Any single continuous structure we tested overestimates the height of the Citsulo segment, whereas two deep faults (a 65-km long northern fault striking 156° and a 30-km long southern fault striking 158°), separated by the Citsulo discontinuity, better fit surface observations (RMSE ~4 m) and require a smaller amount of slip (Figure 4b). The peaks and troughs in scarp height from all simulations broadly match the observations at the surface,

suggesting that the surface displacement is influenced by the near-surface fault geometry (e.g., Mildon et al., 2016; Zielke et al., 2015).

More complex models might fit surface observations better; however, our calculations confirm that the BMF surface expression is not compatible with a deep structure whose strike is perpendicular to the current E-W regional extension direction (Saria et al., 2014) but is compatible with upward propagation of a buried NW-SE striking weak zone (e.g., Worthington & Walsh, 2016).

5. Conclusions

Analysis of a high-resolution DEM and field observations suggests that the scarp of the ~110-km long BMF, Malawi, comprises six 10- to 40-km long segments. The scarp averages 14 m in height but in places exceeds 25 m. This suggests that either multiple earthquake events have ruptured the segments or a continuous rupture with an extraordinarily large amount of slip (> 30 m) has occurred. Although the scarp trace parallels the foliation for more than half of the fault length, large sections do not. We propose that the BMF scarp is a surface expression of a weak zone (or zones) at depth that is not well oriented relative to regional extension but whose strike is subparallel to both the average scarp trend and the strike of the largest magnitude earthquake in southern Malawi (the 1989 Salima event). A simple geometrical model does not reject this hypothesis and indicates that BMF scarp height is likely influenced by the near-surface fault geometry, where locally well oriented metamorphic foliations are reactivated in preference over growth of new faults. Our findings are in agreement with others for north Malawi and elsewhere along the East African Rift System and suggest that deep, weak structures cause a reorientation of the local stress field. These conclusions highlight the importance of considering three-dimensional relationships over a range of length scales when interpreting fault scarps mapped at the surface.

Acknowledgments
The data used are listed in the references, tables, and supporting information. M. H. is supported by the NERC GW4+ Doctoral Training Partnership (grant code NE/L002434/1) and Centre for Observation and Modelling of Earthquakes, Volcanoes and Tectonics (COMET). J. B. is supported by COMET, the NERC Large Grant Looking into Continents from Space (LiCS, NE/K010913/1), and the EPSRC Global Challenges PREPARE (EP/P028233/1). A. F. is supported by the European Research Council (ERC) grant agreement 715836 "MICA" and EPSRC PREPARE. H. M. acknowledges the Geological Survey Department, Malawi, for attaching him to the project. We thank D. Delvaux, H. Fossen, K. McCaffrey, D. Kier, and the anonymous reviewers for constructive comments on the manuscript. TanDEM-X data were obtained via DLR proposal DEM_GEOL0686.

References

Anders, M. H., & Schlische, R. W. (1994). Overlapping faults, intrabasin highs, and the growth of normal faults. *The Journal of Geology*, *102*(2), 165–179. https://doi.org/10.1086/629661

Arrowsmith, J. R., Rhodes, D. D., & Pollard, D. D. (1998). Morphologic dating of scarps formed by repeated slip events along the San Andreas Fault, Carrizo Plain, California. *Journal of Geophysical Research*, *103*(B5), 10,141–10,160.

Avouac, J.-P. (1993). Analysis of scarp profiles: Evaluation of errors in morphologic dating. *Journal of Geophysical Research*, *98*(B4), 6745–6754.

Bellahsen, N., & Daniel, J. M. (2005). Fault reactivation control on normal fault growth: An experimental study. *Journal of Structural Geology*, *27*(4), 769–780. https://doi.org/10.1016/j.jsg.2004.12.003

Bellahsen, N., Leroy, S., Autin, J., Razin, P., D'Acremont, E., Sloan, H., et al. (2013). Pre-existing oblique transfer zones and transfer/transform relationships in continental margins: New insights from the southeastern Gulf of Aden, Socotra Island, Yemen. *Tectonophysics*, *607*, 32–50. https://doi.org/10.1016/j.tecto.2013.07.036

Biggs, J., Nissen, E., Craig, T., Jackson, J., & Robinson, D. P. (2010). Breaking up the hanging wall of a rift-border fault: The 2009 Karonga earthquakes, Malawi. *Geophysical Research Letters*, *37*, L11305. https://doi.org/10.1029/2010GL043179

Cartwright, J. A., Mansfield, C., & Trudgill, B. (1996). The growth of normal faults by segment linkage. *Geological Society, London, Special Publications*, *99*(1), 163–177. https://doi.org/10.1144/GSL.SP.1996.099.01.13

Chorowicz, J., & Sorlien, C. (1992). Oblique extensional tectonics in the Malawi Rift, Africa. *Geological Society of America Bulletin*, *104*(8), 1015–1023. https://doi.org/10.1130/0016-7606(1992)104<1015:OETITM>2.3.CO;2

Claringbould, J. S., Bell, R. E., Jackson, C. A.-L., Gawthorpe, R. L., & Odinsen, T. (2017). Pre-existing normal faults have limited control on the rift geometry of the northern North Sea. *Earth and Planetary Science Letters*, *475*, 190–206. https://doi.org/10.1016/j.epsl.2017.07.014

Collettini, C., Niemeijer, A., Viti, C., & Marone, C. (2009). Fault zone fabric and fault weakness. *Nature*, *462*(7275), 907–10. https://doi.org/10.1038/nature08585

Collettini, C., & Sibson, R. H. (2001). Normal faults, normal friction? *Geology*, *29*(10), 927–930. https://doi.org/10.1130/0091-7613(2001)?029<0927:NFNF>?2.0.CO

Corti, G. (2009). Continental rift evolution: From rift initiation to incipient break-up in the Main Ethiopian Rift, East Africa. *Earth-Science Reviews*, *96*(1-2), 1–53. https://doi.org/10.1016/j.earscirev.2009.06.005

Corti, G., Philippon, M., Sani, F., Keir, D., & Kidane, T. (2013). Re-orientation of the extension direction and pure extensional faulting at oblique rift margins: Comparison between the Main Ethiopian Rift and laboratory experiments. *Terra Nova*, *25*(5), 396–404. https://doi.org/10.1111/ter.12049

Crider, J. G., & Pollard, D. D. (1998). Fault linkage: Three-dimensional mechanical interaction faults. *Journal of Geophysical Research*, *103*(B10), 24,373–24,391.

Crone, A. J., & Haller, K. M. (1991). Segmentation and the coseismic behavior of basin and range normal faults: Examples from east-central Idaho and southwestern Montana, U.S.A. *Journal of Structural Geology*, *13*(2), 151–164. https://doi.org/https://doi.org/10.1016/0191-8141(91)90063-O

Dawers, H., & Anders, M. H. (1995). Displacement-length scaling and fault linkage. *Journal of Structural Geology*, *17*(5), 607–614.

Dawson, A., & Kirkpatrick, I. (1968). The geology of the Cape Maclear peninsula and Lower Bwanje valley. *Bulletin of the Geological Survey, Malawi*, *28*, 71.

Delvaux, D., & Barth, A. (2010). African stress pattern from formal inversion of focal mechanism data. *Tectonophysics*, *482*, 105–128. https://doi.org/10.1016/j.tecto.2009.05.009

Delvaux, D., Kervyn, F., Macheyeki, A., & Temu, E. (2012). Geodynamic significance of the TRM segment in the East African Rift (W-Tanzania): Active tectonics and paleostress in the Ufipa plateau and Rukwa basin. *Journal of Structural Geology*, *37*, 161–180. https://doi.org/10.1016/j.jsg.2012.01.008

Ebinger, C., Rosendahl, B., & Reynolds, D. (1987). Tectonic model of the Malawi rift, Africa. *Tectonophysics*, *141*, 215–235.

Fazlikhani, H., Fossen, H., Gawthorpe, R. L., Faleide, J. I., & Bell, R. E. (2017). Basement structure and its influence on the structural configuration of the northern North Sea rift. *Tectonics*, *36*, 1151–1177. https://doi.org/10.1002/2017TC004514

Fossen, H., & Rotevatn, A. (2016). Fault linkage and relay structures in extensional settings—A review. *Earth-Science Reviews*, *154*, 14–28. https://doi.org/10.1016/j.earscirev.2015.11.014

Gawthorpe, R. L., & Hurst, J. M. (1993). Transfer zones in extensional basins: Their structural style and influence on drainage development and stratigraphy. *Journal of the Geological Society*, *150*, 1137–1152.

Gruber, A., Wessel, B., Huber, M., & Roth, A. (2012). Operational TanDEM-X DEM calibration and first validation results. *ISPRS Journal of Photogrammetry and Remote Sensing*, *73*, 39–49. https://doi.org/10.1016/j. isprsjprs.2012.06.002

He, C., Luo, L., Hao, Q. M., & Zhou, Y. (2013). Velocity-weakening behavior of plagioclase and pyroxene gouges and stabilizing effect of small amounts of quartz under hydrothermal conditions. *Journal of Geophysical Research: Solid Earth*, *118*, 3408–3430. https://doi.org/10.1002/jgrb.50280

Jackson, J., & Blenkinsop, T. (1993). The Malawi earthquake of March 10, 1989: Deep faulting within the East Africa Rift System. *Tectonics*, *12*(5), 1131–1139.

Jackson, J., & Blenkinsop, T. (1997). The Bilila-Mtakataka fault in Malawi: An active, 100-km long, normal fault segment in thick seismogenic crust. *Tectonics*, *16*(1), 137–150.

Kim, Y.-S., & Sanderson, D. J. (2005). The relationship between displacement and length of faults: A review. *Earth-Science Reviews*, *68*(3-4), 317–334. https://doi.org/10.1016/j.earscirev.2004.06.003

Kolawole, F., Atekwana, E. A., Laó-Dávila, D. A., Abdelsalam, M. G., Chindandali, P. R., Salima, J., & Kalindekafe, L. (2018). Active deformation of Malawi Rift's North Basin hinge zone modulated by reactivation of pre-existing Precambrian shear zone fabric. *Tectonics*, *37*, 1–22. https://doi.org/10.1002/2017TC004628

Laó-Dávila, D. A., Al-Salmi, H. S., Abdelsalam, M. G., & Atekwana, E. A. (2015). Hierarchical segmentation of the Malawi Rift: The influence of inherited lithospheric heterogeneity and kinematics in the evolution of continental rifts. *Tectonics*, *34*, 2399–2417. https://doi.org/10.1002/2015TC003953

Lyons, R. P., Scholz, C. A., Buoniconti, M. R., & Martin, M. R. (2011). Late Quaternary stratigraphic analysis of the Lake Malawi Rift, East Africa: An integration of drill-core and seismic-reflection data. *Palaeogeography, Palaeoclimatology, Palaeoecology*, *303*, 20–37. https://doi.org/10.1016/j.palaeo.2009.04.014

Macgregor, D. (2015). History of the development of the East African Rift System: A series of interpreted maps through time. *Journal of African Earth Sciences*, *101*, 232–252.

Mackenzie, D., & Elliott, A. (2017). Untangling tectonic slip from the potentially misleading effects of landform geometry. *Geosphere*, *13*(4), 1310–1328. https://doi.org/10.1130/GES01386.1

McClay, K., & Khalil, S. (1998). Extensional hard linkages, eastern Gulf of Suez, Egypt. *Geology*, *26*(6), 563–566. https://doi.org/10.1130/0091-7613(1998)026<0563:EHLEGO>2.3.CO;2

Mildon, Z. K., Roberts, G. P., Faure Walker, J. P., Wedmore, L. N., & McCaffrey, K. J. (2016). Active normal faulting during the 1997 seismic sequence in Colfiorito, Umbria: Did slip propagate to the surface? *Journal of Structural Geology*, *91*, 102–113. https://doi.org/10.1016/j.jsg.2016.08.011

Morewood, N. C., & Roberts, G. P. (2001). Comparison of surface slip and focal mechanism slip data along normal faults: An example from the eastern Gulf of Corinth, Greece. *Journal of Structural Geology*, *23*, 473–487. https://doi.org/10.1016/S0191-8141(00)00126-7

Morley, C. K. (2002). A tectonic model for the Tertiary evolution of strike-slip faults and rift basins in SE Asia. *Tectonophysics*, *347*(4), 189–215. https://doi.org/10.1016/S0040-1951(02)00061-6

Morley, C. K. (2010). Stress re-orientation along zones of weak fabrics in rifts: An explanation for pure extension in 'oblique' rift segments? *Earth and Planetary Science Letters*, *297*, 667–673. https://doi.org/10.1016/j.epsl.2010.07.022

Nicol, A., Walsh, J., Berryman, K., & Nodder, S. (2005). Growth of a normal fault by the accumulation of slip over millions of years. *Journal of Structural Geology*, *27*, 327–342. https://doi.org/10.1016/j.jsg.2004.09.002

Peacock, D. (2002). Propagation, interaction and linkage in normal fault systems. *Earth-Science Reviews*, *58*, 121–142. https://doi.org/10.1016/S0012-8252(01)00085-X

Pennacchioni, G., & Mancktelow, N. S. (2007). Nucleation and initial growth of a shear zone network within compositionally and structurally heterogeneous granitoids under amphibolite facies conditions. *Journal of Structural Geology*, *29*(11), 1757–1780. https://doi.org/10.1016/j.jsg.2007.06.002

Phillips, T. B., Jackson, C. A., Bell, R. E., Duffy, O. B., & Fossen, H. (2016). Reactivation of intrabasement structures during rifting: A case study from offshore southern Norway. *Journal of Structural Geology*, *91*, 54–73. https://doi.org/10.1016/j.jsg.2016.08.008

Saria, E., Calais, E., Stamps, D. S., Delvaux, D., & Hartnady, C. J. H. (2014). Present-day kinematics of the East African Rift. *Journal of Geophysical Research: Solid Earth*, *119*, 3584–3600. https://doi.org/10.1002/2013JB010901

Scholz, C. (2002). *The mechanics of earthquakes and faulting*. New York: Cambridge University Press.

Tommasi, A., & Vauchez, A. (2001). Continental rifting parallel to ancient collisional belts: An effect of the mechanical anisotropy of the lithospheric mantle. *Earth and Planetary Science Letters*, *185*(1-2), 199–210.

Trudgill, B., & Cartwright, J. (1994). Relay-ramp forms and normal-fault linkages, Canyonlands National Park, Utah. *Geological Society of America Bulletin*, *106*(9), 1143–1157.

Twiss, R. J., & Unruh, J. R. (1998). Analysis of fault slip inversions: Do they constrain stress or strain rate? *Journal of Geophysical Research*, *103*, 12,205–12,222. https://doi.org/10.1029/98JB00612

Villamor, P., & Berryman, K. (2001). A late quaternary extension rate in the Taupo Volcanic Zone, New Zealand, derived from fault slip data. *New Zealand Journal of Geology and Geophysics*, *44*(2), 243–269. https://doi.org/10.1080/00288306.2001.9514937

Walker, R. T., Wegmann, K. W., Bayasgalan, A., Carson, R. J., Elliott, J., Fox, M., et al. (2015). The Egiin Davaa prehistoric rupture, central Mongolia: A large magnitude normal faulting earthquake on a reactivated fault with little cumulative slip located in a slowly deforming intraplate setting. *Seismicity, Fault Rupture and Earthquake Hazards in Slowly Deforming Regions*, *432*, 187–212. https://doi.org/10.1144/SP432.4

Walsh, J. J., Nicol, A., & Childs, C. (2002). An alternative model for the growth of faults. *Journal of Structural Geology*, *24*(11), 1669–1675. https://doi.org/10.1016/S0191-8141(01)00165-1

Walshaw, R. D. (1965). The geology of the Ncheu-Balaka area. *Bulletin of the Geological Survey, Malawi*, *19*, 96.

Whipp, P. S., Jackson, C. a. L., Gawthorpe, R. L., Dreyer, T., & Quinn, D. (2014). Normal fault array evolution above a reactivated rift fabric: A subsurface example from the northern Horda Platform, Norwegian North Sea. *Basin Research*, *26*(4), 523–549. https://doi.org/10.1111/bre.12050

Worthington, R. P., & Walsh, J. J. (2016). Timing, growth and structure of a reactivated basin-bounding fault. *Geological Society of London, Special Publications*, *439*, 511–531.

Zielke, O., Klinger, Y., & Arrowsmith, J. R. (2015). Fault slip and earthquake recurrence along strike-slip faults—Contributions of high-resolution geomorphic data. *Tectonophysics*, *638*(1), 43–62. https://doi.org/10.1016/j. tecto.2014.11.004